Spin-dependent properties in zigzag graphene nanoribbons with phenyl-edge defects

Leandro Salemi,[*] Aurélien Lherbier, and Jean-Christophe Charlier

Institute of Condensed Matter and Nanosciences, Université catholique de Louvain, B-1348 Louvain-La-Neuve, Belgium

Recent outbreaks in bottom-up chemical techniques have demonstrated the synthesis of atomically perfect zigzag graphene nanoribbons (ZGNRs) and of their corresponding analogs with phenyl-edge functionalization [P. Ruffieux *et al.*, Nature **531**, 489 (2016)]. Since spin-polarized currents can be generated at the edges of the ZGNRs, the control of phenyl decoration at the zigzag edges could accurately tune the electronic properties of these carbon-based nanoribbons. In the present paper, using first-principles calculations and a Landauer-Büttiker approach, the electronic and magnetic properties as well as the spin-resolved transmissions are investigated in various phenyl-edge-modified ZGNRs. The understanding of the spin-dependent transport properties in relation to the atomic structure opens the way to design devices such as spin valves for future spintronics applications.

I. INTRODUCTION

Generation and transport of spin-polarized currents are crucial issues for spintronics devices [1]. While ferromagnetic metallic materials have been used to generate such polarized currents, they are not really suited for spin transport as their high spin-orbit coupling leads to fast spin relaxation.

Since the discovery of graphene in 2004, huge scientific interest has aroused around this monoatomic bidimensional layer [2]. Graphene could be suited for a wide range of applications, including spintronics [3]. The eligibility of graphene as a top-class material for spintronics essentially comes from the two following facts: (1) the Fermi velocity of Dirac fermions in graphene is high ($v_F \approx c/300$) [4] and (2) the intrinsic spin-orbit coupling in carbon is weak compared to metallic compounds, leading to long spin-diffusion length ($\sim$10 μm experimentally at room temperature [5]). Theoretical models predict the spin relaxation time τ_s to be around 1 μs [5] although only smaller lifetimes on the order of 100 ps have presently been measured [6–10]. This discrepancy between experiments and theoretical predictions can be explained using unconventional spin relaxation mechanisms such as resonant scattering by magnetic impurities or pseudospin-driven spin-relaxation mechanisms [11,12].

Unfortunately, the lack of intrinsic magnetism in graphene rules out its use for spin-polarized current generation. One could use ferromagnetic electrodes as intermediates for spin injection but the efficiency of such setup has been shown to be inadequate due to important contact-induced spin-relaxation phenomena [7].

Finite strips of graphene, usually referred to as *graphene nanoribbons* (GNRs), display peculiar properties because of low-dimensionality-induced quantum confinement [13–20] and could represent an interesting alternative for spin-transport. Indeed, while armchair GNRs (AGNRs) do not dis-play magnetic ordering, edge-localized magnetic states have been predicted in zigzag GNRs (ZGNRs) [21]. However, as these localized states are extremely sensitive to edge roughness [22], their experimental observation has remained a real challenge for a long time.

Recent outbreaks in bottom-up methods, where atomically precise ribbons where produced, have allowed for a better understanding of such graphene-based 1D structures [23–27]. Edge-localized states were observed at 5 K for ZGNRs [28,29], suggesting that magnetic ordering might be achieved in real systems. Edge engineering, with atomically controlled processes, could then open a route to tailor the spin-dependent properties of these ZGNRs. For example, using self-assembly of well-suited monomers on a gold surface, Ruffieux *et al.* [29] managed to produce and observe such edge-modified structures [see Fig. 1(b)]. As illustrated in Fig. 1(a), the monomer used would at first glance yield a perfectly periodic 1D structure. However, during the cyclodehydrogenation process, these phenyl groups undergo ring closure, which can happen in two directions, inducing aperiodic nanostructures. The defects are strictly localized along the edges and do not modify the global structure of the ribbon. Since edge-localized states are responsible for the magnetic properties of ZGNRs, the effect associated with the occurrence of these edge-defects might lead to interesting spin-dependent transport properties.

In the present paper, the spin-transport properties of *phenyl-edge-modified* 6-ZGNRs (PEM 6-ZGNRs) are investigated using first-principles calculations and a Landauer-Büttiker approach. The simulations suggest that the phenyl groups induce a lowering of the spin-polarization of the carbon atoms localized close to the edge-defect and also introduce spin-dependent scattering centers.

II. METHODS

The electronic structure are computed using density-functional theory method as implemented in SIESTA [30–32]. The exchange-correlation energy and electron-ion

---

[*]Present address: Department of Physics and Astronomy, Uppsala University; leandro.salemi@physics.uu.se
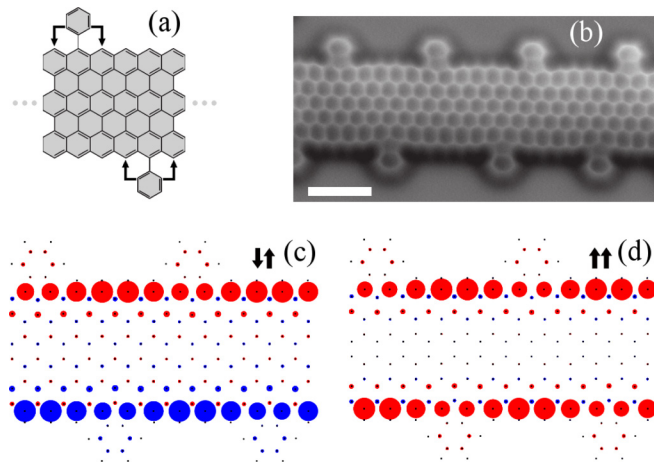
FIG. 1. (a) Periodic 6-ZGNRs with phenyl-edge defects before cyclodehydrogenation as obtained by combining the monomer experimentally produced by Ruffieux *et al.* [29]. This structure is not stable and during the cyclodehydrogenation process, the phenyl groups undergo ring close, falling either on one or the other side. (b) Constant-height nc-AFM frequency shift image of a phenyl-edge modified 6-ZGNR produced with bottom-up techniques. Scale bar is 1 nm. Adapted from Ref. [29]. (c), (d) Spatial distribution of the spin-population difference for the PEM 6-ZGNRs whose unit cell is displayed at Fig. 2(a). In (c), the edge configuration is ↑↓ while in (d) it is ↑↑. If the circle is red (blue), spin-↑ (↓) are majority. The larger the circle, the bigger the spin population. Near the phenyl groups, the spin polarization is effectively reduced.

interaction are described using GGA-PBE [33] functional and norm-conserving pseudopotentials [34] in the fully nonlocal form. A double-ζ polarized basis set of numerical atomic orbitals is used and the energy cutoff for the real-space mesh is set to 200 Ry. The energy levels are populated following a Fermi-Dirac distribution function with an electronic temperature of 300 K. The reciprocal space sampling is performed using a Monkhorst-Pack grid [35] with at least 24 k-points along the transport direction of the pristine 6-ZGNRs. For larger systems, the sampling is adjusted so that the product between the number of 6-ZGNRs equivalent unit cells and the number of k-points would not be less than 24. An interlayer vacuum distance of ∼30 Å is used to avoid any spurious image interactions. All atomic structures are relaxed using a conjugated gradient algorithm until the forces on each atom are less than 0.01 eV/Å.

The calculations are performed using spin-polarized density, neglecting the weak carbon spin-orbit coupling. Two different spin configurations are considered: the antiferromagnetic (↑↓) and ferromagnetic (↑↑) edge polarizations [see Figs. 1(c) and 1(d)], representing the two magnetic states. In each of these configurations, the magnetic ordering along a given edge is ferromagnetic. Spin relaxation is allowed throughout the self-consistent calculations. Therefore, such magnetic states are believed to be stable in the sense that they lay on a local energy minimum. In general, the ↑↓ configuration is found to be more stable than the ↑↑, as discussed further on. To label the two different electronic populations, the following convention is used: the majority population is referred to as spin-↑ (spin-up) electrons while spin-↓ (spin-

TABLE I. Energy differences between the two magnetic configurations ↓↑ and ↑↑ for different (PEM) 6-ZGNR structures ($\Delta E_1 = E_{\uparrow\uparrow} - E_{\uparrow\downarrow}$) and between the nonmagnetic configuration and the ↓↑ configuration ($\Delta E_2 = E_{nm} - E_{\uparrow\downarrow}$). In both cases, a positive number means that the ↑↓ configuration is more stable.

Structure	ΔE_1 [meV/nm]	ΔE_2 [meV/nm]
Pristine 6-ZGNRs	57	307
PEM 6-ZGNRs [Fig. 2(a)]	19	101
PEM* 6-ZGNR [Fig. 3(a)]	36	212
PEM** 6-ZGNR [Fig. 3(c)]	38	223
PEM** 6-ZGNR [Fig. 3(e)]	31	258

down) electrons refers to the minority one. Note that in the case of spin-degeneracy, even if there is no majority/minority population, we will still refer to ↑ electrons and ↓ electrons.

The quantum transport calculations are performed under the nonequilibrium Green's functions (NEGF) formalism as implemented in TranSIESTA [36]. The physical system is described by three different parts. The first two parts are the right and left leads, which are considered semi-infinite. Those two leads do not need to be the same but periodicity is required. They are accounted through the so-called self-energies. The last part is called the scattering region and is the finite part of our system, often containing scattering centers. To study the effect of different geometries of edge-defects on the transport spectra, we used pristine 6-ZGNRs as left and right leads (see insets of Fig. 3). In the case of a pristine 6-ZGNR/PEM 6-ZGNR junction, a pristine 6-ZGNR is used for the left lead while a PEM 6-ZGNR is used for the right one [see Fig. 4(a)].

III. RESULTS

As shown in Table I, we observe that all (PEM) 6-ZGNR structures considered are found to be more stable in the ↑↓ configuration than in the ↑↑ one. This goes in the same direction as other works found in the literature [37–41]. Table I also shows the energy difference between the nonmagnetic state and the antiferromagnetic state. For high-density of phenyl-edge defects, a decrease of ∼60% is observed while for lower density the decrease is less than ∼30%. The magnetic ↑↓ configuration stays in all cases favorable.

The PEM 6-ZNGRs synthesized in Ref. [29] are characterized by a random distribution of the phenyl groups along the zigzag edge. More specifically, the randomness lays in the spacing between two neighboring phenyl-edge defects. However, the number of different topologies is quite restrained since the phenyl defects can only be separated by three, four, or five pristine zigzag cusps. To perform practical electronic structure calculations, a periodic structure along the ribbon axis is considered [see Fig. 2(a)].

The electronic band structure of a PEM 6-ZGNRs in the ↑↓ configuration is displayed in Fig. 2(b) and compared to the pristine case (dashed lines). Both edges are topologically equivalent and the structure possesses a glide plane so that the spin degeneracy is preserved. The inclusion of phenyl defects along the edges open gaps at the Brillouin zone (BZ) boundaries. The openings do not affect drastically the energy
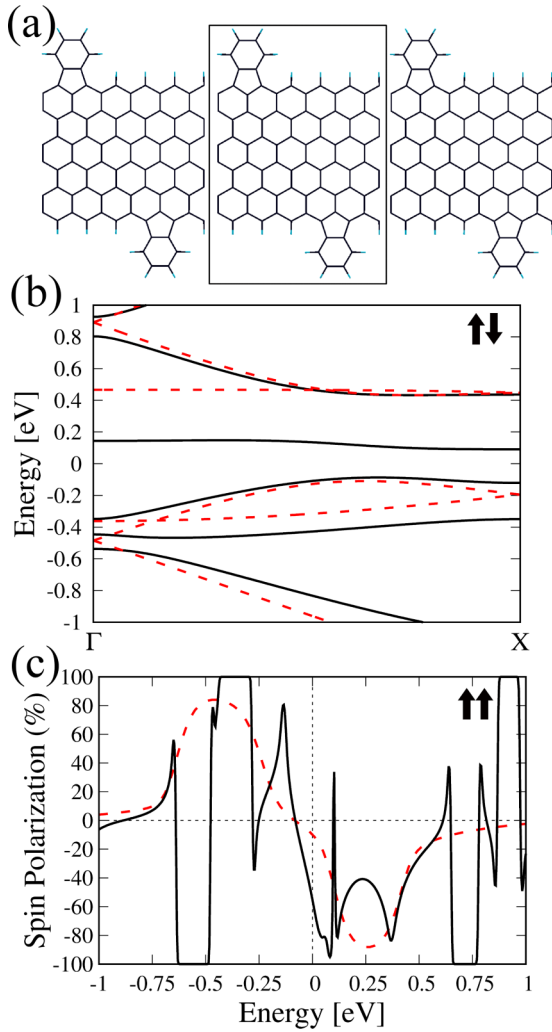
FIG. 2. (a)Schematic of a PEM 6-ZGNR structure. The unit cell is represented by the black box. (b) Band structure of the PEM 6-ZGNR in the $\uparrow\downarrow$ configuration (black). The red dashed line represents the electronic band structure of pristine 6-ZGNR shifted of 140 meV toward higher energies. The states are spin degenerate. The inclusion of phenyl defects open gaps at the BZ boundaries $\mathbf{k} \rightarrow X$. As a result, a localized state around $90-150$ meV above the Fermi energy appears. Omitting this state, the band gap is around 520 meV. (c) Spin polarization for the PEM 6-ZGNR (black) and for the pristine 6-ZGNR (red dashed line) as defined in Eq. (1). Around -0.5 eV and 0.75 eV, an abrupt switching between only $\uparrow/\downarrow$ states arises for the PEM structure. This feature is not to be seen in pristine 6-ZGNRs and is remarkable as it may lead to fully spin-polarized electronic currents.

dispersion except for the conduction band where one part of it is shifted toward $90-150$ meV above the Fermi energy. The stabilization of this nearly nondispersive state is mediated by the π_z orbitals carried by the phenyl groups [42]. This state is thus strongly associated with the edge-defect concentration. Indeed, it becomes more spatially localized around the phenyl groups as the concentration of the phenyl defects is lowered. Omitting this "localized" state, the band gap of the PEM 6-ZNGR is predicted to be around 520 meV while pristine 6-ZGNRs have a band gap of $\sim$540 meV. As shown later, this localized state does not play any role in the conduction properties of the PEM(*) 6-ZGNRs investigated in the present work.

In the $\uparrow\uparrow$ configuration, spin degeneracy is lifted and a net magnetic moment of $\sim$2.52 μ_B is estimated. Pristine 6-ZGNRs of equivalent length would hold a magnetic moment of 2.6 μ_B. Therefore, the presence of phenyl groups along the edges effectively decreases the magnetization, as illustrated in Figs. 1(c) and 1(d), where the spin polarization around the carbon atoms at the edge close to the defects is clearly reduced.

Since the spin degeneracy is lifted in the $\uparrow\uparrow$ configuration, the spin polarization $\mathcal{P}(E)$ can be quantified:

$$\mathcal{P}(E) = \frac{N_\uparrow(E) - N_\downarrow(E)}{N_\uparrow(E) + N_\downarrow(E)}, \tag{1}$$

where $N_\uparrow(E)$ ($N_\downarrow(E)$) is density of states for a spin $\uparrow$ ($\downarrow$) electron. If $\mathcal{P}(E)$ is equal to 100% (-100%), the system is said to be fully polarized.

As illustrated in Fig. 2(c), a fully polarized system occurs for specific windows of energies such as around $E = [-0.7; -0.5]$ eV, $[-0.4; -0.3]$ eV, and $[0.65; 0.7]$ eV. This behavior suggests that those structures might exhibit spin-filtering characteristics for spin carriers at these specific energies. The spin polarization around $E = -0.5$ eV is especially interesting as the system switches quite abruptly from fully $\uparrow$-polarized to fully $\downarrow$-polarized. Since this feature is not seen in the pristine case [see red dashed line in Fig. 2(c)], we can say that it arises because of the inclusion of phenyl-edge defects.

To investigate the influence of the phenyl groups on the spin transport, three different edge configurations of finite-length PEM(*) 6-ZGNRs are considered, each with pristine 6-ZGNRs as leads [see Figs. 3(a), 3(c) and 3(e)]. The two first structures (PEM* and PEM** 6-ZGNRs) are referred to as the *symmetric structures* [insets of Figs. 3(a) and 3(c)] while the last one (PEM*** 6-ZGNR) is referred to as the *one-sided modified structure* [inset of Fig. 3(e)].

For the symmetric structures in the $\uparrow\downarrow$ configuration [Figs. 3(a) and 3(c)], while quantitative differences are observed, both conductances exhibit qualitatively similar features. The most remarkable difference is the dip in the conductance around $E = -0.48$ eV, which is larger when the opposed phenyl groups are further from each other. Other calculations actually show that the dip in the conductance increases as opposing defects are further apart. The gaps are also observed to be larger than the pristine case (dashed lines), which can be explained by a global shift of the electronic chemical potential due to the edge defects. Indeed, as mentioned in the previous section, the width of the gap is barely affected by the phenyl groups. However, the valence and conduction band are shifted by $\sim$0.1 eV toward higher energies, leading to an effectively larger transport gap for the devices as the conductance is suppressed up to $E = 0.36$ eV ($E = 0.28$ eV for pristine 6-ZGNRs). The localized midgap state mentioned earlier does not participate in the transport as it falls inside the transport gap. Finally, as spin degeneracy is preserved, no net spin current is observed.

In the $\uparrow\uparrow$ configurations [Figs. 3(b) and 3(d)], both spin channels follow approximately the same trends outside
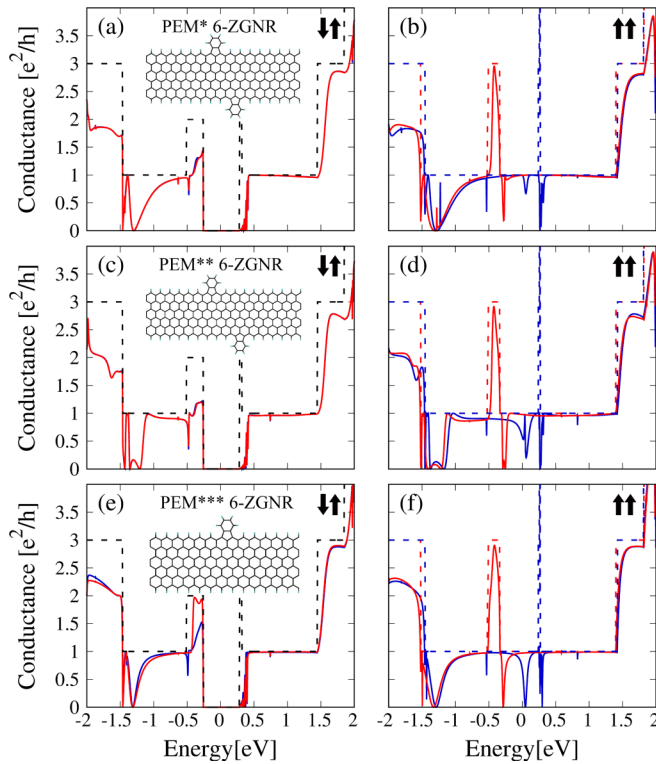
FIG. 3. Spin-resolved transmission spectra for 6-ZGNRs with various configurations of phenyl groups at their edges. The figures are paired as the left one shows the spectrum for the ↑↓ while the right one the spectrum for the ↑↑. The insets of the ↑↓ spectra show the geometrical configuration considered. The red (blue) line represents the spin-↑ (↓) electrons. The dashed lines are for pristine 6-ZGNR. (a) PEM* 6-ZGNR, (c) PEM** 6-ZGNR, (e) PEM*** 6-ZGNR.

FIG. 4. (a) Setup of a junction between semi-infinite pristine 6-ZGNR and semi-infinite PEM 6-ZGNRs. The leads are represented in blue. They are considered to be semi-infinite within the NEGF method. (b) Transmission spectrum in the ↑↓ configuration. (c) Transmission spectrum in the ↑↑ configuration. The red (blue) curve depicts the spin-↑ (↓) electrons.

the range $[-1; 1]$ eV. Inside this energy window, the high conductance for spin ↑ electrons around $E = -0.4$ eV is only slightly affected by the defects in both symmetric structures. This zone of high conductance is slightly narrower than in pristine ribbons and the nicely quantized plateau has become a relatively wide peak. In addition, a well in the conductance for spin-↓ electrons right above the Fermi energy is predicted. At the energy of the overshoot (~ 0.25 eV) in the conductance of spin-↓ electrons for pristine 6-ZGNRs, a strange behavior of the spin-↓ electrons is observed as the conductance decreases and recovers drastically, requiring further investigation.

The one-sided modified structure displays properties which are tightly related to the symmetric structures. Indeed, in the ↑↓ configuration [Fig. 3(e)], the spin-↓ channel is similar to what has been observed for the symmetric structures. The similarity is especially noticeable around $E = -0.5$ eV, where the sharp decrease in conductance suggests that back-scattering is enhanced. This resonant energy is only relevant for electrons whose spin is associated with the polarization of the defected edge (i.e., the spin-↑ conduction channel does not experience enhanced backscattering at this energy). Consequently, the sharp decrease of the conductance at this resonant energy can be considered as a characteristic signature of edges exhibiting phenyl-group functionalization. As the spin degeneracy is lifted, spin-polarized current, which would mainly

be hole-mediated, may be achieved. For spin-↑ electrons, the quantized plateau at $2e^2/h$ in the range $[-0.5; -0.25]$ eV is nearly preserved although its width is slightly reduced since it starts at $E = -0.4$ eV. This effect is due to the shift in electronic chemical potential induced by the single phenyl group at the unique functionalized edge.

In the ↑↑ configuration [Fig. 3(f)], both spin channels follow the same trends outside the range $[-1; 1]$ eV, as for the symmetric case. Inside this energy window, the respective conduction of both spin-↑ and spin-↓ electrons goes to zero at two specific energies. For the spin-↑ electrons, extinction happens at $E = -0.3$ eV while for the spin-↓ channel the conductance drops to zero about 50 meV above the Fermi energy. Such features are of technological interest as small voltages might lead to highly polarized currents, inducing possible spin-filtering applications. Hence, even if statistically difficult to produce by combining pristine and phenyl functionalized monomers, a long one-sided PEM*** 6-ZGNR, with all the phenyl defects only along one edge, would pin the magnetism on one of its edge as a result of the spin depletion mentioned above. Such a structure would offer a way of controlling the magnetism at the edge of the device with consequently asymmetric magnetic moments. For spin transmission, the development of efficient spin valves by tuning the gate voltage to achieve complete spin channel extinctions is still an important issue for spintronics application.

In this last section, a junction between pristine 6-ZGNR and PEM 6-ZGNR is proposed [see Fig. 4(a)]. Such structure could possibly be synthesized by alternating two different monomers during a two-step bottom-up synthesis.

The study of such a specific carbon-based nanojunction is essentially motivated by the following two facts. First, in the ↑↑ configuration, the availability of electronic states for the PEM 6-ZGNRs becomes zero for one spin while staying finite for the other one [see Fig. 2(c)], suggesting possible spin-filtering characteristics. Second, in the ↑↓ configuration, a global shift is observed in the band diagram, strongly

indicating that a junction between pristine 6-ZGNR and PEM 6-ZGNR would lead to a *pn* junction. Since 6-ZGNR will play the role of the n-type semiconductor, a transition between n/p regions would occur on the atomic scale.

The spin-dependent transport properties of this *pn* junction are presented in Figs. 4(b) and 4(c). In the ↑↓ configuration, the transmission is found to be nearly spin degenerated [see Fig. 4(b)]. The structure is semiconducting, with a transport gap of ∼0.7 eV. As explained before, this enlargement compared to the band gap of the pristine 6-ZGNR is due to a shift in the electronic chemical potential. This effect also leads to a misalignment of the pristine and PEM 6-ZGNRs conduction (valence) band minima (maxima). Compared to the previous case of symmetric pristine leads [i.e., n-p-n junction in Figs. 3(a) and 3(c)], one notes that the sharp dip at E = −0.5 eV has become a gap, and that two other transport gaps appear around $E = -1.25$ and 0.8 eV.

In the ↑↑ configuration, spin degeneracy is strongly lifted and multiple transport gaps appear for each spin channel. From −0.64 eV to −0.47 eV, the spin-↑ channel undergoes complete extinction while the spin-↓ channel displays a finite conductance of e^2/h [see Fig. 4(c)]. From −0.44 eV to −0.28 eV, the opposite situation occurs and the conductance for spin-↓ electrons goes to zero while the one for spin-↑ electrons lays between $2e^2/h$ and $3e^2/h$.

Such a feature would suggest using this nanojunction as a spin-filtering device where the spin current could switch its polarization for a small variation of the bias voltage. Therefore, the challenge consists of displacing the Fermi level toward an energy range of ∼0.5 eV. If this can be achieved in such a nanojunction, small bias voltages could drain fully polarized currents.

IV. DISCUSSION

As demonstrated in the previous section, phenyl-edge defects might be used to tailor the spin-dependent properties of ZGNRs. One of the biggest challenges lays in the existence of the magnetic states and in the stabilization of one ordering over the other. The first issue is partially solved by the increasing number of bottom-up techniques that allow for the synthesis of precise nanostructures. The stabilization problem is more critical as the energy differences between the two magnetic configurations are of the same magnitude than thermal fluctuations at room temperature. However, this lower energy difference could also allow weaker magnetic fields to pin the edge magnetism. This could be advantageous as the ↑↑ configuration also exhibits interesting features.

Using bottom-up techniques, both the 6-ZGNRs and the PEM 6-ZGNRs were successfully synthesized by Ruffieux *et al.* [29]. The availability of monomers for both structures suggests that the realization of a pristine 6-ZGNR/PEM 6-ZGNR junction might be achievable. Since both ribbons are produced under similar conditions as the polymerization is thermally induced on by the aryl-aryl coupling of halogen functions, one could then imagine pumping the first-used monomer out of the reaction chamber and injecting the second one to further polymerize. The copolymerization of both monomers also shows some perspectives where the statis-

tical distribution of pristine and PEM 6-ZGNRs along the nanostructure could be controlled by the relative abundance of the monomers.

In this work, the case of free-standing nanostructures has been investigated. In practice, such structures lay on a substrate that affects their electronic properties. The effect of the inclusion of a gold substrate has been investigated at by Shinde *et al.* [42]. In general, the structural properties of the ribbon are found to be unaffected by the substrate while electronic properties are quite impacted.

As we focused our work on experimentally produced structures, the effect of the width of the ribbon on spin-transport properties has not been explicitly investigated. However, comparing Figs. 3(a) and 3(b) with Figs. 3(c) and 3(d), we notice that the relative distance between phenyl defects on opposite edges has an influence on the transmission spectra. This suggests that ribbons as narrow as 6-ZGNRs still have nonzero interactions between edges. Since the edge states, which account for magnetic properties in ZGNRs, are localized, we can expect a decreasing cross-influence between opposite edges as the width of the ribbon increases. However, this goes beyond the scope of this work and requires further investigation.

V. CONCLUSION

In summary, the chemical incorporation of phenyl defects along the edges of the 6-ZGNRs is responsible for the appearance of localized states just above the Fermi energy (↑↓ configuration) and for strong polarization of the available states (↑↑ configuration). A shift toward higher energies of the Fermi level is observed and the total magnetization is found to decrease as the phenyl groups locally deplete the spin population.

The influence of phenyl-edge defects on the spin-resolved transport spectra is far from being negligible. Our results confirm that quantum transport properties of ZGNRs are highly dependent on the edge states and promote the concept of edge-engineering to tailor electronic properties of GNRs.

Notable breakthroughs have been achieved with the development of bottom-up chemistry approaches, where perfectly edged GNRs as well as more complex nanostructures with controlled atomic arrangements [43] are obtained from the assembly of small specific monomers.

The development of accurate computational methods to account for more complex phenomena, e.g., interaction with metallic substrates, will become essential to describe such systems. The key role that computational modeling has to play will be to systematically screen the electronic-transport properties of the nanostructures to suggest devices that will answer the technological challenges of future nano (spin) electronics.

[1] I. Žutić, J. Fabian, and S. Das Sarma, Rev. Mod. Phys. **76**, 323 (2004).

[2] K. S. Novoselov, A. K. Geim, S. V. Morozov, D. Jiang, Y. Zhang, S. V. Dubonos, I. V. Grigorieva, and A. A. Firsov, Science **306**, 666 (2004).

[3] N. Kheirabadi, A. Shafiekhani, and M. Fathipour, Superlattices Microstruct. **74**, 123 (2014).

[4] A. H. Castro Neto, F. Guinea, N. M. R. Peres, K. S. Novoselov, and A. K. Geim, Rev. Mod. Phys. **81**, 109 (2009).

[5] W. Han, R. K. Kawakami, M. Gmitra, and J. Fabian, Nat. Nanotechnol. **9**, 794 (2014).

[6] N. Tombros, C. Jozsa, M. Popinciuc, H. T. Jonkman, and B. J. van Wees, Nature **448**, 571 (2007).

[7] W. Han, K. McCreary, K. Pi, W. Wang, Y. Li, H. Wen, J. Chen, and R. Kawakami, J. Magn. Magn. Mater. **324**, 369 (2012).

[8] C. Józsa, T. Maassen, M. Popinciuc, P. J. Zomer, A. Veligura, H. T. Jonkman, and B. J. van Wees, Phys. Rev. B **80**, 241403 (2009).

[9] M. Popinciuc, C. Józsa, P. J. Zomer, N. Tombros, A. Veligura, H. T. Jonkman, and B. J. van Wees, Phys. Rev. B **80**, 214427 (2009).

[10] M. Shiraishi, M. Ohishi, R. Nouchi, N. Mitoma, T. Nozaki, T. Shinjo, and Y. Suzuki, Adv. Funct. Mater. **19**, 3711 (2009).

[11] D. Kochan, M. Gmitra, and J. Fabian, Phys. Rev. Lett. **112**, 116602 (2014).

[12] D. V. Tuan, F. Ortmann, D. Soriano, S. O. Valenzuela, and S. Roche, Nat. Phys. **10**, 857 (2014).

[13] K. Nakada, M. Fujita, G. Dresselhaus, and M. S. Dresselhaus, Phys. Rev. B **54**, 17954 (1996).

[14] K. Wakabayashi, M. Fujita, H. Ajiki, and M. Sigrist, Phys. Rev. B **59**, 8271 (1999).

[15] M. Ezawa, Phys. Rev. B **73**, 045432 (2006).

[16] L. Brey and H. A. Fertig, Phys. Rev. B **73**, 235411 (2006).

[17] K.-i. Sasaki, S. Murakami, and R. Saito, J. Phys. Soc. Jpn. **75**, 074713 (2006).

[18] V. Barone, O. Hod, and G. E. Scuseria, Nano Lett. **6**, 2748 (2006).

[19] L. Yang, C.-H. Park, Y.-W. Son, M. L. Cohen, and S. G. Louie, Phys. Rev. Lett. **99**, 186801 (2007).

[20] N. M. R. Peres, F. Guinea, and A. H. Castro Neto, Phys. Rev. B **73**, 125411 (2006).

[21] Y.-W. Son, M. L. Cohen, and S. G. Louie, Phys. Rev. Lett. **97**, 216803 (2006).

[22] J. Kunstmann, C. Özdoğan, A. Quandt, and H. Fehske, Phys. Rev. B **83**, 045414 (2011).

[23] J. Cai, P. Ruffieux, R. Jaafar, M. Bieri, T. Braun, S. Blankenburg, M. Muoth, A. P. Seitsonen, M. Saleh, X. Feng, K. Müllen, and R. Fasel, Nature **466**, 470 (2010).

[24] J. Björk, S. Stafström, and F. Hanke, J. Am. Chem. Soc. **133**, 14884 (2011).

[25] H. Huang, D. Wei, J. Sun, S. L. Wong, Y. P. Feng, A. H. C. Neto, and A. T. S. Wee, Sci. Rep. **2**, 983 (2012).

[26] S. Linden, D. Zhong, A. Timmer, N. Aghdassi, J. H. Franke, H. Zhang, X. Feng, K. Müllen, H. Fuchs, L. Chi, and H. Zacharias, Phys. Rev. Lett. **108**, 216801 (2012).

[27] T. H. Vo, M. Shekhirev, D. A. Kunkel, M. D. Morton, E. Berglund, L. Kong, P. M. Wilson, P. A. Dowben, A. Enders, and A. Sinitskii, Nat. Commun. **5**, 3189 (2014).

[28] S. Wang, L. Talirz, C. A. Pignedoli, X. Feng, K. Müllen, R. Fasel, and P. Ruffieux, Nat. Commun. **7**, 11507 (2016).

[29] P. Ruffieux, S. Wang, B. Yang, C. Sánchez-Sánchez, J. Liu, T. Dienel, L. Talirz, P. Shinde, C. A. Pignedoli, D. Passerone, T. Dumslaff, X. Feng, K. Müllen, and R. Fasel, Nature **531**, 489 (2016).

[30] E. Artacho, D. Sanchez-Portal, P. Ordejon, A. Garcia, and J. Soler, Phys. Status Solidi B **215**, 809 (1999).

[31] J. Junquera, Ó. Paz, D. Sánchez-Portal, and E. Artacho, Phys. Rev. B **64**, 235111 (2001).

[32] E. Anglada, J. M. Soler, J. Junquera, and E. Artacho, Phys. Rev. B **66**, 205101 (2002).

[33] J. P. Perdew, K. Burke, and M. Ernzerhof, Phys. Rev. Lett. **77**, 3865 (1996).

[34] N. Troullier and J. L. Martins, Phys. Rev. B **43**, 1993 (1991).

[35] H. J. Monkhorst and J. D. Pack, Phys. Rev. B **13**, 5188 (1976).

[36] M. Brandbyge, J.-L. Mozos, P. Ordejón, J. Taylor, and K. Stokbro, Phys. Rev. B **65**, 165401 (2002).

[37] G. Z. Magda, X. Jin, I. Hagymási, P. Vancsó, Z. Osváth, P. Nemes-Incze, C. Hwang, L. P. Biró, and L. Tapasztó, Nature **514**, 608 (2014).

[38] J. Jung and A. H. MacDonald, Phys. Rev. B **79**, 235433 (2009).

[39] M. Fujita, K. Wakabayashi, K. Nakada, and K. Kusakabe, J. Phys. Soc. Jpn. **65**, 1920 (1996).

[40] H. Lee, Y.-W. Son, N. Park, S. Han, and J. Yu, Phys. Rev. B **72**, 174431 (2005).

[41] L. Pisani, J. A. Chan, B. Montanari, and N. M. Harrison, Phys. Rev. B **75**, 064418 (2007).

[42] P. P. Shinde, O. Gröning, S. Wang, P. Ruffieux, C. A. Pignedoli, R. Fasel, and D. Passerone, Carbon **124**, 123 (2017).

[43] A. Lherbier, L. Liang, J.-C. Charlier, and V. Meunier, Carbon **95**, 833 (2015).